ANALYSIS OF THERMAL-HYDRAULIC GRAVITY/ BUOYANCY EFFECTS IN THE TESTING OF THE ITER POLOIDAL FIELD FULL SIZE JOINT SAMPLE (PF-FSJS)

R. Zanino[1], P. Bruzzone[2], D. Ciazynski[3], M. Ciotti[4], P. Gislon[4], S. Nicollet[3] and L. Savoldi Richard[1]

[1] Dipartimento di Energetica, Politecnico
Torino, I-10129, Italy

[2] EPFL-CRPP, Euratom-Swiss Association
Villigen PSI, CH-5232, Switzerland

[3] Association Euratom-CEA, CEA/Cadarache
St Paul Lez Durance Cedex, F-13108, France

[4] Euratom-ENEA Association, Frascati Research Center
Frascati, I-00044, Italy

ABSTRACT

The PF-FSJS is a full-size joint sample, based on the NbTi dual-channel cable-in-conduit conductor (CICC) design currently foreseen for the International Thermonuclear Experimental Reactor (ITER) Poloidal Field coil system. It was tested during the summer of 2002 in the Sultan facility of CRPP at a background peak magnetic field of typically 6 T. It includes about 3 m of two jointed conductor sections, using different strands but with identical layout. The sample was cooled by supercritical helium at nominal 4.5-5.0 K and 0.9-1.0 MPa, in forced convection from the top to the bottom of the vertical configuration. A pulsed coil was used to test AC losses in the two legs resulting, above a certain input power threshold, in bundle helium backflow from the heated region. Here we study the thermal-hydraulics of the phenomenon with the M&M code, with particular emphasis on the effects of buoyancy on the helium dynamics, as well as on the thermal-hydraulic coupling between the wrapped bundles of strands in the annular cable region and the central cooling channel. Both issues are ITER relevant, as they affect the more general question of the heat removal capability of the helium in this type of conductors.

CP710, *Advances in Cryogenic Engineering: Transactions of the Cryogenic Engineering Conference - CEC, Vol. 49,* edited by J. Waynert et al.

INTRODUCTION

The PF-FSJS [1] was built using two full-size straight conductors (legs), cabled by Europa Metalli and jacketed by Ansaldo, according to the ITER 2-channel (annular cable bundle "B" and central channel "H" regions) cable-in-conduit concept (see FIG 1). The cable is compacted in a thick SS jacket, according to the ITER PF design [2]. The conductor consists of 1152 strands, cabled in a 3×4×4×4×6 pattern. Each leg uses NbTi strands with different resistive barrier, leading to different inter-strand resistances and therefore different AC losses. The total length (~ 3.5 m) of each leg includes two terminations: the upper ones (~ 0.6 m long) are used to connect the sample to the independently cooled bus bars of the test facility, while the lower ones (also ~ 0.6 m long) are joined together to close the electric circuit [1]. From the thermal-hydraulic point of view, the two legs are cooled independently with supercritical helium in forced-flow, nominally at 4.5-5.0 K and 0.9-1.0 MPa.

The PF-FSJS was tested in the Sultan facility of CRPP Villigen, Switzerland in 2002 [3]. Here we concentrate mainly on the AC loss tests of the right leg (the left leg exhibited similar behavior). During the field pulse, the highest temperature was recorded *upstream* of the AC field, when the input power was above a certain threshold. First explanations of the phenomenon were proposed, stressing the role of the gravity force in the helium dynamics [4], as well as emphasizing the importance of the thermal-hydraulic coupling between the two helium channels [5], but a detailed modeling of the whole transient was not carried out.

In this paper we model the thermal-hydraulic phenomenon with the M&M code [6] and we present the results of the simulations of some of the AC loss shots, comparing them also with a resistively heated shot.

EXPERIMENTAL SETUP

The PF-FSJS sample configuration is sketched in FIG 1. Both right and left legs are instrumented with five temperature sensors: T2, T3 [1], and T4 are glued in Cu blocks brazed on the conductor jacket, T1 is inserted in the helium flow in the bundle region of the conductor, while T5 is mounted on the outlet helium pipe. The mass flow rate dm/dt along each leg is measured downstream of the sample. During all runs considered here, it was always regulated in feed back loop in order to keep it about constant – an important constraint here, but not relevant in the case of a coil. Two heat sources are available on each leg: 1) a resistive heater (OH) is wrapped around an ~ 0.4 m long portion of the conductor jacket with reduced thickness, upstream of T2; 2) a pulsed coil provides a variable magnetic field over a length of ~ 0.39 m inducing AC losses, between T2 and T4. Thick SS clamps (not shown in FIG 1) with epoxy insulation are applied all along the two legs, with the only exception of the temperature sensor locations, and of the OH region [1].

RESULTS AND ANALYSIS

M&M Model. Upgrade and Calibration Issues

The effect of gravity was included in the M&M model [6] in the form of the following two contributions: 1) The respective body force, $\rho_j\, g \cos(\varphi)$, is added to the total (dynamic + static) pressure gradient - $\partial p_j/\partial x$ in the helium momentum equation of each channel j (=

[1] T3 turned out to be not fully reliable during transients and it will not be considered in the following.

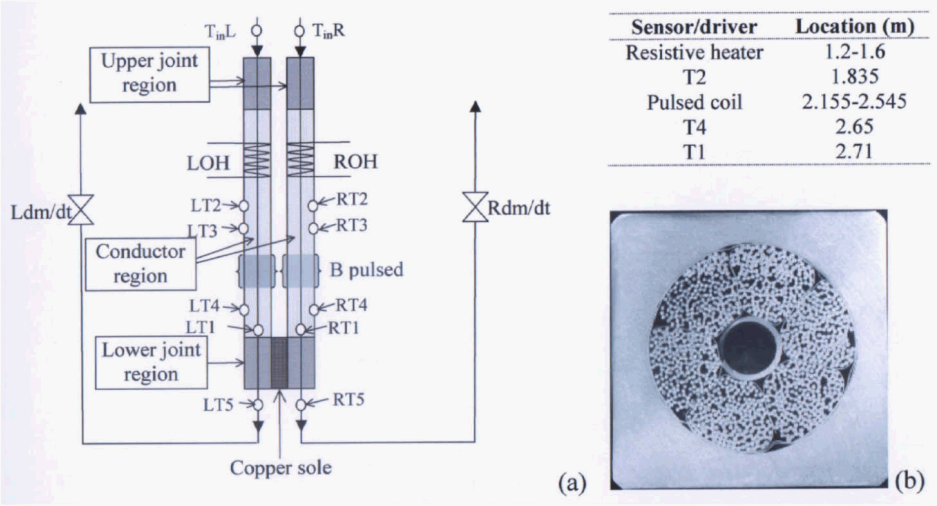

Sensor/driver	Location (m)
Resistive heater	1.2-1.6
T2	1.835
Pulsed coil	2.155-2.545
T4	2.65
T1	2.71

FIGURE 1. The PF-FSJS. (a) Schematic view of the full sample, including major thermal-hydraulic sensors and drivers (locations are given from the inlet of the upper joint). (b) Conductor cross-section (51 mm side).

B, H); 2) The power generated by this force per unit volume, $v_j \rho_j g \cos(\varphi)$, is added to the helium (internal + kinetic) energy equation of each channel. Here, cos(φ) accounts for the angle between the conductor (x coordinate measured from the top) and the direction of the acceleration g, ρ_j is the helium density, v_j is the helium flow speed along each channel.

The classical up-wards buoyancy force arises in the helium due to the combination of gravity and heat deposition, as heated helium expands. This is particularly true for the B helium, which is directly heated by the contact with strands and/or jacket, while the heating of the H helium is only indirect and depends on the amount of coupling between the two channels (see below). If this coupling is not perfect, a transverse temperature gradient will arise in the CICC and buoyancy will lead to strands (and jacket) being locally cooled by natural (or free) convection upwards, while the forced convection is maintained downwards in the central channel. Although the gravity head was long recognized as giving a non-negligible contribution in static conditions (see, e.g., [7]), its dynamic counterpart, i.e., the buoyancy force, is considered here for the first time in the context of ITER CICC, to the best of our knowledge.

In the 2-channel geometry of the CICC we have to cope with continuous heat and mass transfer between the two channels but, unfortunately, there is a lack in basic experimental results to be able to properly model both the conductive and the convective mechanisms (in steady state as well as during transients) in a fully validated fashion. In M&M the difficult and presently open problem of the calibration of heat transfer between B and H is treated including free parameters for each contribution (conductive and convective) to the transverse heat flux $q_\perp = q_\perp^{cond} + q_\perp^{conv}$ (see [8] for details), in the absence of a first principle model/correlation. In $q_\perp^{cond}$, which is driven by the temperature difference $\Delta T_\perp = T_B - T_H$, an ad-hoc multiplier M_{cond} of the series of thermal conductances at the B-H interface is implemented. In this series, the standard Dittus-Boelter correlation for pipes is used for the helium heat transfer coefficient with *any* solid, for the sake of simplicity.[2] For the convective part, the *transverse* mass flow $G_\perp$ (and the corresponding

[2] The corresponding lower bound is set at the laminar value of the Nusselt number Nu = 8.235. Note that this limit is derived from measurements performed with Re>1100 [9], while the values of Re_B in the tests considered here is < 1000. A laminar limit Nu = 4, as for a smooth pipe, was adopted by other authors [10].

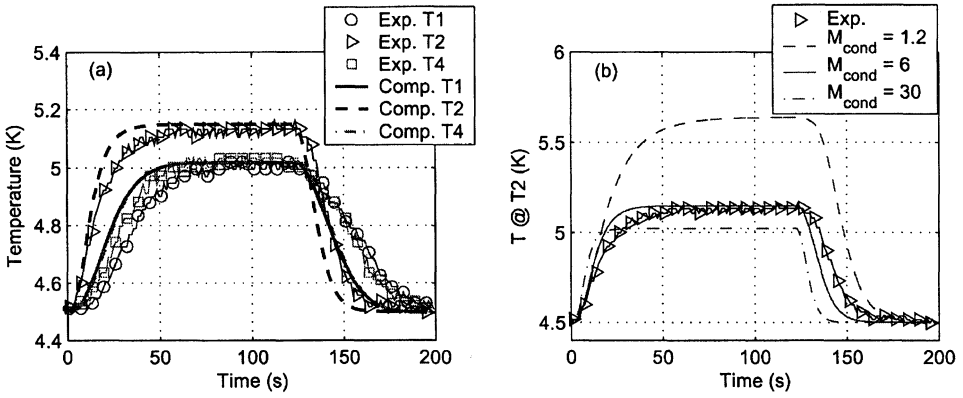

FIGURE 2. Shot WAC130901: (a) Measured T4, T2 and T1 (all base-lined to T4(t=0)), compared to computed temperature evolution. (b) Sensitivity of the computed temperature evolution at T2 to the choice of M_{cond}.

$q_{\perp}^{conv}$), driven by the pressure difference $\Delta p_{\perp} = p_B - p_H$, is modelled like a flow through a valve with ad-hoc "friction factor" K_{conv}. The values of M_{cond} and K_{conv} influence the simulated evolution of the transient and therefore they need to be calibrated for the specific conductor and transients under investigation. A calibration strategy was established in the past and successfully applied to different type of transient, e.g., heat slug [9] and/or quench [10, 11] propagation.

The simulations in this paper have been performed on the right leg of the PF-FSJS, from the inlet of the upper termination to the outlet of the lower joint (heat transfer through the joint is neglected for the sake of simplicity, so that the measured value at T5 cannot be used in the following for comparison). Boundary conditions are: constant inlet pressure p_{in}, inlet temperature T_{in} = T4 (t = 0), and outlet flow speed v_{out} (t) deduced from the measured $(dm/dt)_{out}$ (t) ~ constant. The jacket cross-section variation along the conductor is also included in the model (reduced at the resistive heater, increased everywhere else by a factor of ~ 2.5, to take into account the non-negligible heat capacity of the SS clamps).

Resistively heated shot

We consider first a resistive heater test, shot WAC130901 at 8 g/s, without transport current, where only the right leg was separately heated. The heater was turned on at t = 0 s and turned off at t = 120 s. FIG 2 shows that all temperature sensors react with progressively later, smaller and slower temperature increase, as we move downstream. Using as driver the nominal power in the heater (14 W), deposited fully into the jacket as a square wave in space and time, we compute the evolution of T2, T4, and T1 for different values of K_{conv} and M_{cond}. The best-fit results, obtained with K_{conv} = 5 and M_{cond} = 6, are reported in FIG 2a, showing a very good agreement with the experimental plateau level for all of the three sensors, while the computed ramp-up and down is faster than measured [3]. The parametric effect of M_{cond} variations by a factor of 5, on the evolution of the computed temperature at T2, is shown in FIG 2b. If the B-H coupling is lower (i.e., for lower M_{cond}) then the B helium stays hotter while flowing downstream and a higher plateau is computed at T2. The simulations show no sensitivity to the variation of K_{conv} in the range 2.5-10.

[3] The computed slopes appear to be influenced by the heat capacity of the solid materials, in particular of the clamps (if the clamps were not included in the model, the computed temperature evolutions would look more like square waves) and by the heat transfer coefficient between bundle helium and jacket. The low dm/dt forces h_B to be computed from the laminar lower limit (i.e., h_B is independent of Reynolds in this case).

Simulations performed for this case with vs. without the gravity contribution (not shown) indicate that it has a very small to negligible effect on the computed temperature evolution at the sensors (all downstream of the heater), probably because of the relatively low ratio of input power to mass flow rate in the run at hand (see also below).

Inductively heated shots

Estimation of the input power from AC losses

The correct input power from the AC losses needs to be determined beforehand. We consider a subset of the AC loss shots, WAC220804-07, see TABLE 1, where a pulsed field with a frequency of 2 to 5 Hz was applied on the virgin conductors over a period $t_{pulse} \sim 60$ s, without any transport current. If we assume that no heat is exchanged between right and left leg through the lower joint (see below), the energy E deposited in the right leg during the shot is computed as follows:

$$E = \int dm/dt \times \Delta h_{He} dt = \int dm/dt \times \left(h_{He}(T5(t)) - h_{He}(\langle T5 \rangle) \right) dt \quad (1)$$

where T5(t) is the measured value, $<T5>$ is the average initial value of T5 before the pulse starts, the enthalpy variation Δh_{He} of the helium is computed at a constant pressure p = 1.015 MPa, and the integral runs over the whole transient duration from t = 0, when the AC field is turned on, till a steady state has been reached again after the AC field was turned off (or till the end of the recorded data). From Eq. (1) we can then compute the input power $Q^{low} = E/ t_{pulse}$. Since, however, the different interstrand resistance in the two legs determined higher AC losses and thus higher heat deposition in the right leg [3], the right leg actually cools down by heat transfer through the joint, and Q^{low} represents only a lower bound for the input power. An upper bound Q^{up} can be computed applying Eq. (1) to T1 instead of T5. The input power resulting from the field pulse can thus be estimated as $Q = ½ (Q^{low} + Q^{up}) \pm ½ (Q^{up} - Q^{low})$, as reported in TABLE 1 (an additional contribution to the error bar, not included here, should come from the not recorded tail of the shot, see FIG 3 below).

Analysis of shots WAC220804 - 07

The measured temperature evolution at the different sensors is reported in FIG 3a-d for shots at increasing Q. T4 and T1 are located only 10-15 cm (see FIG 1) downstream of the heated region, and the estimated v_B (t = 0) ~ 1-2 cm/s, so that they take-off very quickly, driven by B helium convection, after the beginning of the heating. On a longer timescale (20-40 s), for Q > ~ 5 W, an increase of the *upstream* T2 is also observed, which can only be interpreted (to be confirmed by the simulations below) as an indication of backflow of hot helium, at least in the bundle region. The backflow is faster, the higher Q is, but the inlet temperature (not shown) remains unperturbed. While all peak temperatures

TABLE 1. Simulated AC loss shots

Shot #	Type	dm/dt (g/s)	Freq (Hz)	t_{pulse} (s)	Max ΔT4 [a] (K)	Max ΔT2 [a] (K)	Power [b] (W)
WAC220804	AC loss at 2 T	4	2.0	60	0.38	0	4.7 ± 0.8
WAC220805	AC loss at 2 T	4	3.0	60	0.57	0.77	8.8 ± 1.0
WAC220806	AC loss at 2 T	4	4.0	60	0.78	1.23	14 ± 1.5
WAC220807	AC loss at 2 T	4	5.0	60	0.98	1.63	18.5 ± 1.6

[a] Maximum temperature increase measured at sensor during the whole transient
[b] Estimated (see text)

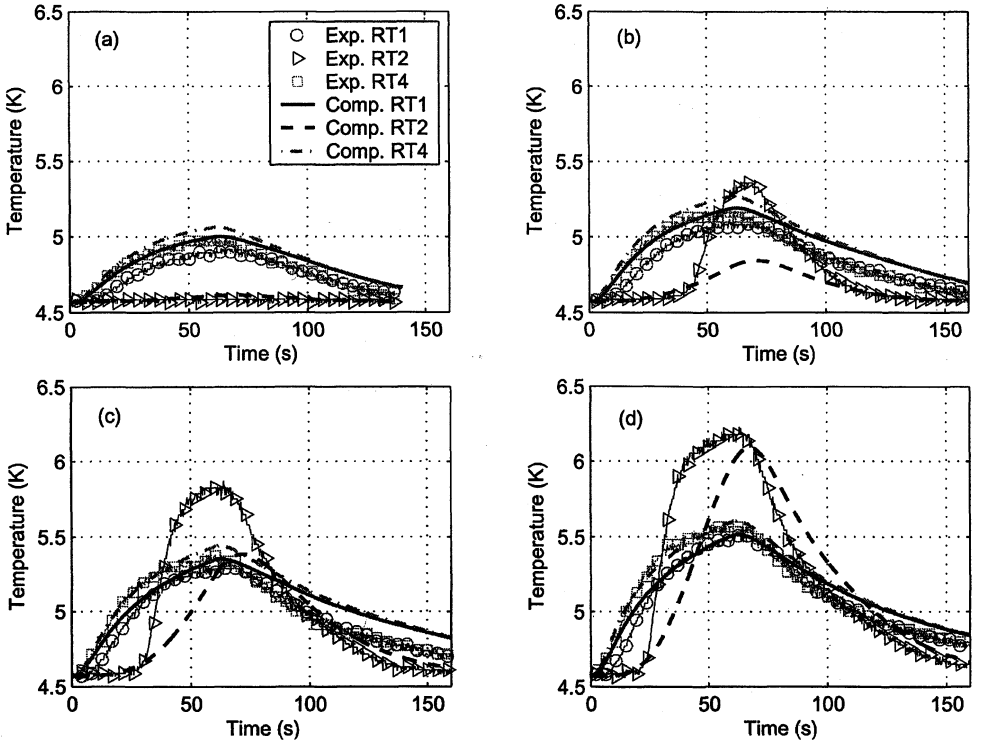

FIGURE 3. Comparison between measured (symbols) and computed (lines) temperature evolutions at T2, T4, T1 in different AC loss runs with increasing Q (see TABLE 1). (a) Shot WAC220804; (b) Shot WAC220805; (c) Shot WAC220806; (d) Shot WAC220807.

increase with Q, the peak T2 is also higher than T4 and T1, although the latter are closer to the heated region, indicating that the directly heated helium moves upward. It may also be noticed that T2 tends to reach a plateau.

In the simulations, the average Q from TABLE 1 has been used for all shots, fed entirely and directly to the strands. A new calibration of the B-H coupling was also performed for this different type of transient. The calibration was aimed at best fitting the peak temperature increase at T2 on shot WAC220807, see FIG 3d, and it led to $K_{conv} = 5$ and $M_{cond} = 1.2$, which are then kept frozen in all AC loss simulations. Note that this value of M_{cond} is a factor of 5 below that needed to best fit the resistive shot above, and that with this value the resistive run simulation would overestimate the measured $\Delta T2$ by a factor ~ 2 (see FIG 2b). Also in this case, however, h_B is independent of Reynolds, i.e., from the mass flow rate. If the dependence on dm/dt would be accounted for, a somewhat lower M_{cond} could be expected, compared to the resistive case. Part of this difference may be related with the above-mentioned uncertainty in the lower bound for Nu, but we do not have at present a full justification for the quantitative difference of M_{cond} needed in the two cases.

The results of the simulation are compared to the measured values in FIG 3. There is good agreement with the experiment in the downstream sensors (T4 and T1) at all Q. Concerning the behavior of the solution upstream, first of all the important feature of the Q threshold for the T2 response (i.e., for backflow) is qualitatively reproduced. The hot rising helium reaches T2 at approximately the correct time, but then the rise of the signal is much slower (more similar to a ramp than to the step-wise shape of the measured temperature) and no plateau is seen in the simulation. Also, the coupling parameter values which allow a

good fit of the peak temperature at T2 for the highest Q do not lead to good quantitative agreement in the case of lower Q, see FIG 3a-c. The fundamental role played by the gravity/buoyancy force in this transient is emphasized by the fact that *no variation of the upstream temperature at T2 nor backflow is seen in simulations without gravity* contribution while, as opposed to the resistive case, also downstream sensors are quantitatively affected (not shown).

In FIG 4 the computed dm/dt(x) and T(x) in the B and H regions are reported at the time when the pulsed coil is turned off (t = 60 s). We note that B helium is being transported upwards starting form the pulsed coil location. In order to maintain the total dm/dt ~ constant, the mass flow rate in the hole has to increase, i.e., helium is being driven from B to H upstream of the heater and backwards to B downstream. As to the temperature profiles, T_B (and therefore the temperature of strands and jacket) is being transported upwards by convection. The heating of the H helium mostly occurs upstream of the heater, i.e., it is mainly due to $q_\perp$, but $\Delta T_H << \Delta T_B$ at the heater, indicating a relative de-coupling between B and H on these short distances.

The parametric effect of M_{cond} variations by a factor of 5, on the evolution of the computed temperature at T2, is shown in FIG 5 (no sensitivity to variations of K_{conv}). The same coupling used for the resistive case (M_{cond} = 6) would lead to no backflow here, a larger coupling apparently implying stronger cooling from the down-flowing H helium and therefore lower reach of the "bubble" upstream. On the contrary, the computed T4 and T1 (not shown) are relatively insensitive to variations of M_{cond} (as the helium flowing downstream of the heater in both regions comes mostly from the hole, see FIG 4).

CONCLUSIONS AND PERSPECTIVE

Thermal-hydraulic transients, induced in the PF-FSJS either by a resistive heater at 8 g/s or by AC losses at 4 g/s, have been analyzed with M&M. The temperatures measured downstream of the heater in the resistive run are well reproduced by the code, assuming in the model a certain level of B-H coupling. Concerning the AC loss tests:

1. The fundamental role of buoyancy forces is such that, in the PF-FSJS, the region where the AC power is deposited is cooled by natural convection (up-wards) against the down-wards flowing helium in forced convection, with a reduction in the heat removal capability of the coolant, at least in terms of the time needed to recover; on the contrary,

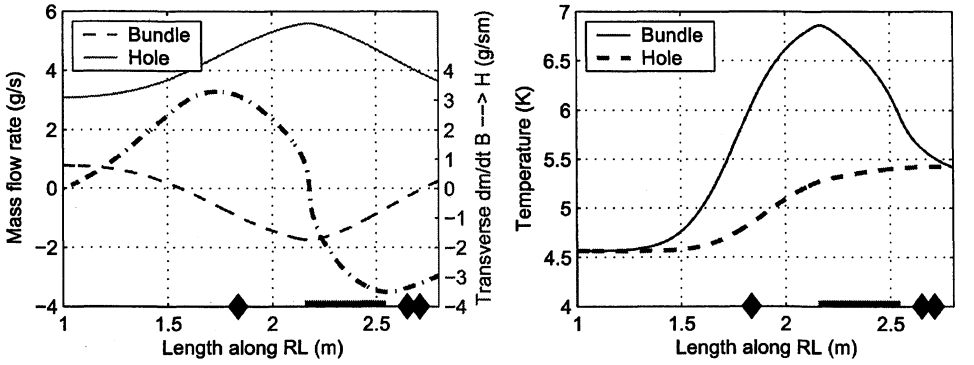

FIGURE 4. Computed spatial profile of the solution for WAC220807 @ t=60s. (a) dm/dt_B (x) (solid line) and dm/dt_H (x) (dashed line), transverse mass flow rate per unit length $G_\perp/L$ (dash-dotted). (b) T_B (x) (solid line) and T_H (x) (dashed line). The location of the sensors (solid diamonds) and of the heated region (solid rectangle) is also reported.

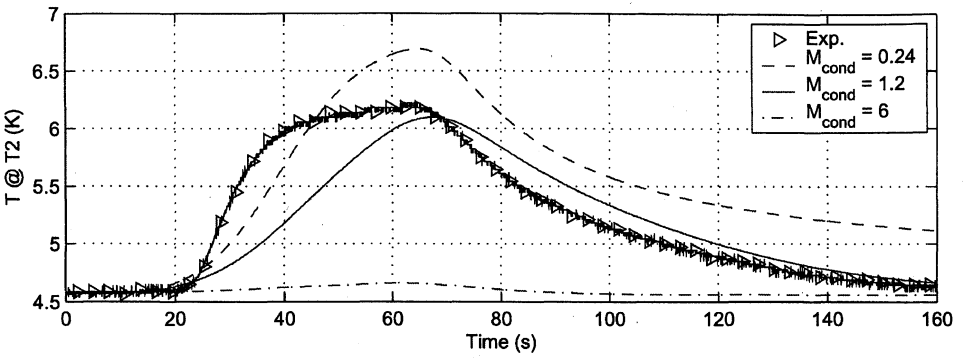

FIGURE 5. Shot WAC220807. Sensitivity of the computed temperature evolution at T2 to the choice of M_{cond}.

forced flow convection in the opposite (up-wards) direction would obviously add-up beneficially;

2. The measured temperature evolution downstream of the AC pulse region is well reproduced by M&M, but upstream the agreement is only qualitative. These difficulties emphasize that there is still insufficient knowledge of transverse heat and mass transfer processes in the typical 2-channel ITER CICC, which affects the accuracy of a detailed modeling.
3. In the extrapolation to ITER coils, no significant contribution of buoyancy to the helium dynamics is expected in the case of the PF and CS, because the slope of the conductor there should be very small. The case of the TF, with partly vertical conductors, significant nuclear heat load, and alternating up-down forced convection in odd-even pancakes, warrants a dedicated investigation, which will be presented elsewhere. Mass flow rate, input power and operating pressure effects should be considered parametrically.

In the perspective, we also plan to study if and how the buoyancy effects analyzed in this paper, and the related nature of the thermal-hydraulic coupling between the two helium channels, affected the stability of the PF-FSJS conductor.

REFERENCES

1. Decool, P., et al., "Design and manufacture of a prototype NbTi full-size joint sample for the ITER poloidal field coils, *Fusion Engineering and Design*, **66-68**, pp. 1165-1169 (2003).
2. Bessette, D., et al., *IEEE Trans. Appl. Supercond.* **11**, pp. 1550-1553 (2001).
3. Ciazynski, D., et al. "Test results of the first 50 kA NbTi full size sample for ITER," presented at EUCAS, Sorrento, Italy (2003).
4. Ciazynski, D., et al., "Test of the PF-FSJS in Sultan. Thermal-hydraulics and calibrations", presented at the CRPP Workshop, Gstaad, Switzerland, January 22-24, 2003.
5. Bruzzone, P., "Remarks on central channel and heat removal", presented at the CRPP Workshop, Gstaad, Switzerland, January 22-24, 2003.
6. Savoldi, L. and Zanino, R., *Cryogenics* **40**, pp. 179-189 (2000).
7. Nicollet, S., et al. Cryogenics **40**, pp. 569-575 (2000).
8. Zanino, R., et al., J. Fus. Energy **14**, pp. 25-40 (1995).
9. Wachi, Y., et al., IEEE Trans. on Appl. Supercond. **5**, pp. 568-571 (1995).
10. Shajii, A., "Theory and modeling of quench in cable-in-conduit superconducting magnets", MIT Report PFC/RR-94-5 (1994).
11. Zanino, R. and Marinucci, C., Cryogenics, **39** pp. 585-593 and 595-608 (1999).
12. Zanino, R., et al., "Computer Simulation of Quench Propagation in QUELL", Adv. Cryo. Eng. 43, pp. 181-188 (1998).
13. Zanino, R., et al., IEEE Trans. Appl. Supercond. **9**, pp. 608-611 (1999).